ARTICLE IN PRESS

Ain Shams Engineering Journal xxx (xxxx) xxx

Contents lists available at ScienceDirect

Ain Shams Engineering Journal

journal homepage: www.sciencedirect.com

“Calculation of onset voltage of corona over a solid dielectric surface encasing rod-rod gap”

Mohamed I. Awaad *, Ahmed N. Tahoon, Mahmoud M. El-Bahy

Department of Electrical Engineering, Benha Faculty of Engineering, Benha University, Benha 13511, Egypt

ARTICLE INFO

Article history:
Received 6 November 2022
Revised 7 January 2023
Accepted 15 February 2023
Available online xxxx

Keywords:
Rod-rod gap encased by a solid dielectric cylinder
Gas-insulated system (GIS)
Electric field calculation
Charge simulation method (CSM)
Streamer inception criterion
SF_6-N_2 mixtures

ABSTRACT

In a gas-insulated system, when the stressed conductors are encased by a solid dielectric, the corona onset voltage (COV) over its surface increases, minimizing the corona discharge. The paper's objective is to calculate the positive COV over the surface of a solid dielectric cylinder that encased rod-rod gap with a common axis and by shifting the two axes a certain distance. This calls for calculating the Laplacian electric field using the charge simulation method. The streamer inception criterion is used to calculate the positive COV at the dielectric surface for surrounding gases SF_6, air, CO_2, N_2, argon and SF_6-N_2 mixture. The equivalences between the COV of SF_6 and the proposed SF_6-N_2 mixture were performed at different pressures and dielectric thicknesses to allow confident use as an alternative insulation to SF_6. The electric field and COV results agree well with the previously published values calculated by software COMSOL and those measured experimentally, respectively.

1. Introduction

In gas-insulated systems (GIS), the solid dielectric is used to insulate HV conductors. It plays the role of supporting material, isolating the gas chamber, and insulating different potential metal parts. Conductors in GIS may be covered with a solid dielectric to insert high-resistive elements for gas-discharge paths. A cross-section of a typical configuration of an industrial HV support insulator encasing rod-rod gap is given in Fig. 1. It is described as a mechanical shaft used to transmit mechanical motion across different potentials [1,2]. It shows two rod-rod gap configurations; sample (a), a solid dielectric cylinder encasing a rod-rod gap with a common axis, sample (b), a solid dielectric cylinder encasing a rod-rod gap by shifting the two axes a certain distance. Fig. 1 sample (a) shows a well-defined location of a high field region around the perimeter of the dielectric cylinder in the surrounding gas due to the difference between the permittivity of the gas and solid dielectric. By shifting the axis of the rod-rod gap, the high field region is enhanced and localized on one side of the dielectric cylinder. The electric field enhancement over the surface of the solid dielectric influences the corona inception in the high field region. When the electric field over the solid dielectric surface reaches a critical value, corona discharge can be initiated. The streamer inception criterion has been widely used in literature to predict the COV at the solid dielectric surface [3–7]. The conditions necessary for the initiation of streamer discharge were applied to obtain the critical strength of the background field and the corresponding COV. Streamer discharge results in partial deterioration of the solid dielectric requiring equipment repair or even its replacement [8]. Therefore, the insulation design highly requires knowledge of the COV at the gas–solid dielectric interface. HV equipment should be designed so the COV is higher than its normal operating voltage.

SF_6 possesses excellent insulating properties, which makes it widely used in GIS. However, it has a drawback that adversely affects the environment since it is a potent greenhouse gas. Intense research has been published to find alternative insulation to SF_6 that has a lesser impact on the environment and comparable dielectric [9–17]. Unfortunately, the liquefaction temperature of all investigated gases is high [18–19]. To decrease the liquefaction temperature, SF_6 is mixed with N_2. To reduce the use of SF_6 to the most, a suitable SF_6-N_2 mixture substitutes SF_6 for developing environmentally friendly HV devices. Getting a suitable SF_6-N_2 mixture with a solution to the SF_6 usage drawbacks would be possible. The possibility of adopting the 50% SF_6 + 50% N_2 mixture as a standard gas option for gas-insulated transformers, gas-insulated transmission lines, and HV circuit breakers was studied. This mixture operated at 15% higher pressures exhibits the same dielectric strength as pure SF_6. The same mixture was listed as having 0.88

* Corresponding author.
E-mail addresses: Mohamed.awad@bhit.bu.edu.eg (M.I. Awaad), Ahmed.Nasreldeen@bhit.bu.edu.eg (A.N. Tahoon), mmbahy@bhit.bu.edu.eg (M.M. El-Bahy).

https://doi.org/10.1016/j.asej.2023.102209

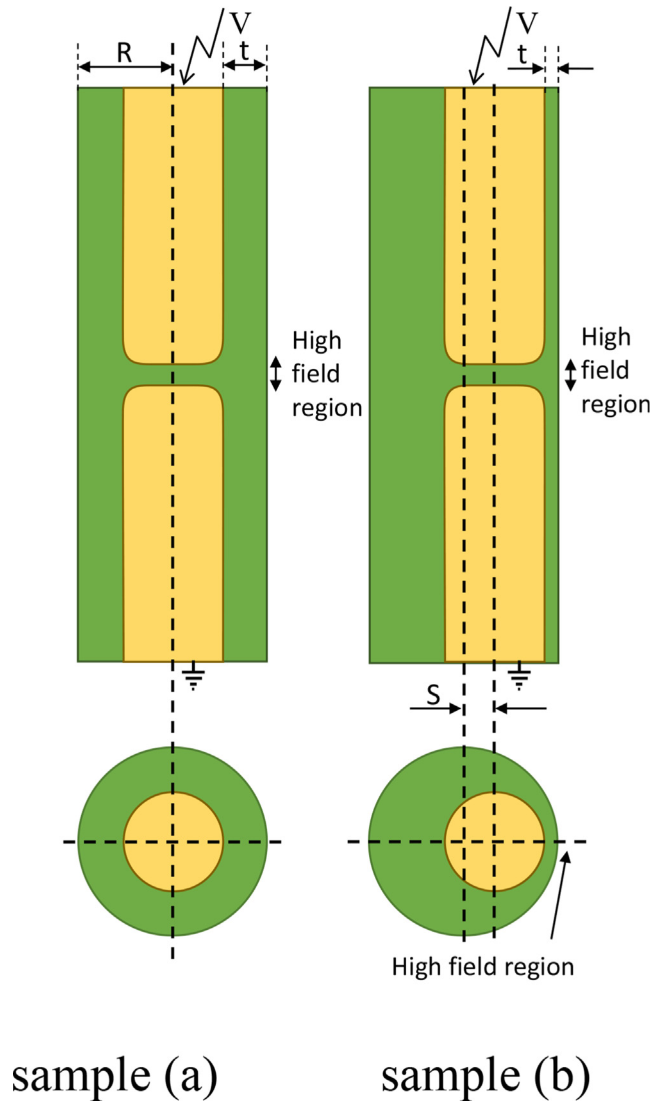

Fig. 1. Investigated samples, length L, solid dielectric cylinder radius R, rod radius r, gap length G.

the dielectric strength of pure SF_6 at the same pressure and a condensation point 20 °C lower [11].

This paper aims to calculate the positive COV over a solid dielectric surface encasing rod-rod gap. By applying HV AC, the peak voltage value is chosen as a reference value since it determines the maximum field stress, which is responsible for the inception of corona discharge. Positive COV is calculated for electronegative gases (SF_6, SF_6-N_2 mixtures, air, and CO_2) and electropositive gases (N_2 and argon). This study is conducted to calculate the positive COV using SF_6-N_2 mixtures at the solid dielectric-gas interface. Streamer criterion is used for COV calculation. This calls for accurate field calculation in the vicinity of a solid dielectric surface using CSM [20–27]. The electric field is accurately calculated for a solid dielectric cylinder encasing rod-rod gap with a common axis and shifting the two axes at a certain distance. Fictitious ring charges are used for simulating the surface charges of the two gap configurations. Due to the asymmetry of the solid dielectric cylinder in sample (b), ring charges with variable charge density are used to simulate the surface charge over the solid dielectric [27]. In addition, the electric field is accurately calculated for a rod-rod gap without the solid dielectric. The calculated values of field and COV over the solid dielectric surface are compared with those calculated before by the software COMSOL 5.2. and measured experimentally before, respectively [1,2] and found to be coinciding.

2. Method of analysis

2.1. calculation of electric field

The analysis is based on the CSM [20–27]. The distributed charges on the surface of the rods are simulated by a set of fictitious ring charges arranged inside the rods. However, the surface charge on the interface between two dielectrics is simulated by two sets of ring charges on both sides of the dielectric interface. Satisfaction of pertinent boundary conditions, namely, the Dirichlet condition at the surface of rods and the Neumann condition at the dielectric surface, results in a set of equations whose simultaneous solution determines the unknown ring charges. Knowing the simulation ring charges, the electric potential and field can be calculated at any point in the investigated geometry.

2.1.1. Simulation of surface charge on a solid dielectric cylinder encasing rod-rod gap

Sample (a): A solid dielectric cylinder encasing rod-rod gap with a common axis.

Fig. 2 sample (a) shows the solid dielectric cylinder encasing rod-rod gap with a common axis. The rod-rod gap is stressed by an applied voltage V. The distribution of charges on the surface of each rod is simulated by three sets of ring charges distributed uniformly inside each rod (Fig. 2 (a)). The 1st set n_1, the 2nd set n_2 and the 3rd set n_3 simulate each rod's flat, rounded and cylindrical parts. Hence, the number of distributed charges on each rod surface = N, (=n_1 + n_2 + n_3). All ring charges simulating the surface charge of the rods are placed inside it at an envelope distant a_1 from its surfaces.

In the solid dielectric, the dipoles are aligned by the electric field, resulting from the voltage, V and compensate each other through the dielectric volume, leaving net charges at the interface between the dielectric and the surrounding gas. Two sets of ring charges simulate these surface charges. Each set has M ring charges uniformly distributed, one placed inside the dielectric at an envelope distant A_1 from the dielectric surface and the other placed in the surrounding gas at an envelope distant A_1 from the dielectric surface. Subsequently, the total number of simulation charges equals 2 N + 2 M. Two sets of boundary points are selected to estimate the simulation charges: one on the rods' surfaces and the other on the interface between the dielectric and surrounding gas. The distance between two successive boundary points is a_0 on the rods' surfaces and A_0 on the dielectric surface.

Sample (b): A solid dielectric cylinder encasing rod-rod gap with shifting the two axes a certain distance.

The simulation of surface charges on each rod is the same as explained before in sample (a). As explained before, the net charges at the interface between the solid dielectric and the surrounding gas are simulated by two sets of ring charges. To account for the asymmetry created by the presence of shift distance S in axes, as shown in Fig. 1 sample (b), simulation ring charges with variable charge density are considered. Each ring is assumed to be divided into 2n segments, and the charge density remains constant over the segment, Fig. 2 (b). The segment length is assumed variable; to be minimum in the high field region and increases gradually around half of the periphery of the ring. Hence, the number of simulation charges for the solid dielectric cylinder is 2n times 2 M. Subsequently, the number of simulation charges for the investigated geometry equals (2 N + 2n $\times$ 2 M). The number of segments is taken as a function of the offset distance S, n $= integer(f_1 S)$,

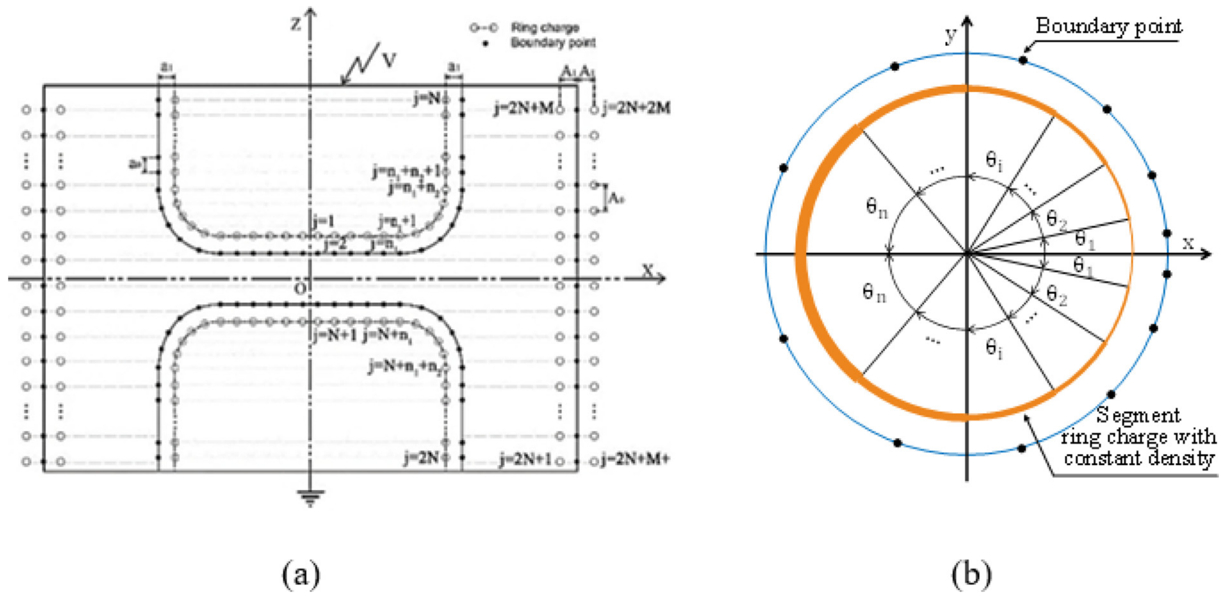

Fig. 2. (a) Distribution of simulation charges for sample (a). (b) Division of ring charge along their entire perimeter into 2n ring segments.

$\theta_1 = \frac{\pi}{\sum_{i=1}^{i=n} f_2^{i-1}}$, $\theta_i = f_2^{i-1}\theta_1$, where, f_1 and f_2 are arbitrary constants, i = 1, 2, ….., n. The distance between two successive boundary points remains a_0 on the rods' surfaces and A_0 on the solid dielectric surface.

For sample (a), the simulation accuracy is affected by the number of simulating ring charges 2 N + 2 M and their location depending on the parameters a_0, a_1, A_0 and A_1. The sample length, L, is taken as $f_0 \times L$, where $f_0 > 1$. In addition, for sample (b), the accuracy is also affected by the arbitrary constants f_1 and f_2 and the 2n number of ring segments with variable charge density.

Charge simulation of rod-rod gap without solid dielectric

The rod-rod gap used above is stressed by an applied voltage V. The charges on the rods' surfaces are simulated by the same ring charges described before in sample (a). Hence, the number of simulation ring charges = 2 N.

2.1.2. Calculation of the unknown simulation charges

To determine the simulation charges, pertinent boundary conditions must be satisfied at the chosen boundary points. These boundary conditions are explained as follows:

(i) The potential, φ, calculated at any boundary point on the rods' surfaces, is the algebraic sum of the potentials at this point produced by the simulation ring charges of the rods and the surrounding gas. The potential, φ, must be equal to the applied voltage V for the HV rod and zero for the grounded rod. i.e.

$$\varphi_i = \sum_{j=1}^{2N} P_{ij}Q_j + \sum_{j=2N+M+1}^{2N+2M} P_{ij}Q_j = V_i, i = 1, 2, \cdots, 2N\# \qquad (1)$$

(ii) Two boundary conditions are satisfied at each boundary point A(x, z) on the interface between the solid dielectric and the surrounding gas. At any point on the interface, when it is seen from the solid dielectric side, the potential φ_1 is the algebraic sum of potentials at this point due to the simulation charges of the rods' surfaces and the surrounding gas. The potential φ_2, is the algebraic sum of the potentials at this point due to the simulation charges of the rods' surfaces and the solid dielectric cylinder [20–26], if the point is seen from the gas side. As the potential is continuous, φ_1 and φ_2 should be equal, i.e.

$$\sum_{j=1}^{2N} P_{ij}Q_j + \sum_{j=2N+M+1}^{2N+2M} P_{ij}Q_j = \sum_{j=1}^{2N+M} P_{ij}Q_j, i = 2N+1, \cdots, 2N+M\# \qquad (2)$$

(iii) En1 and En2 are the normal components of the field, at any boundary point A(x, z) when seen from the solid dielectric and the gas sides, respectively. They are related to each other through the relative permittivity, ε_r, of the solid dielectric to satisfy the continuity of electric flux in the direction normal to the dielectric interface [20–26]. These field components are calculated using the simulation charges used in calculating the potentials φ_1 and φ_2, respectively.

$$\varepsilon_r\left(\sum_{j=1}^{2N} Fn_{ij}Q_j + \sum_{j=2N+M+1}^{2N+2M} Fn_{ij}Q_j\right) = \left(\sum_{j=1}^{2N+M} Fn_{ij}Q_j\right),$$
$$i = 2N+1, \cdots, 2N+M\# \qquad (3)$$

Satisfaction of the boundary conditions using equations (1) - (3) applied at the respective boundary points A(x, z) results in a set of simultaneous equations (4) whose solution determines the unknown simulation charges.

$$\begin{bmatrix} P & 0 & P \\ 0 & -P & P \\ (\varepsilon_r - 1)F_n & -F_n & (\varepsilon_r)F_n \end{bmatrix} \begin{bmatrix} Q_1 \\ \vdots \\ Q_N \\ Q_{N+1} \\ \vdots \\ Q_{2N} \\ Q_{2N+1} \\ \vdots \\ Q_{2N+M} \\ Q_{2N+M+1} \\ \vdots \\ Q_{2N+2M} \end{bmatrix} = \begin{bmatrix} V \\ \vdots \\ V \\ 0 \\ \vdots \\ 0 \\ 0 \\ \vdots \\ 0 \\ 0 \\ \vdots \\ 0 \end{bmatrix} \qquad (4)$$

where, P and F_n are the potential and normal field coefficients of a simulation charge calculated at a boundary point A(x, z) [20–26].

For constant density ring charge, the potential and the field coefficients are given in [20,21 25, 26]. For variable density segmented ring charge, the potential and the field coefficients are given in [27]. The electric field and potential can be calculated at any point in the gas and the dielectric cylinder when the simulation charges are known for the investigated geometry.

2.1.3. Calculation of potential and electric Field

The potential, φ_1(x, z), the radial and axial components, Ex_1(x, z) and Ez_1(x, z), and the absolute field E_1(x, z) at a point A(x, z) located on the rods' surfaces or in the solid dielectric are expressed by equations (5–8). They are the sum of the potentials, the radial-and axial-field components produced at this point by the simulation charges of the rods, and the surrounding gas:

$$\varphi_1(x,z) = \sum_{j=1}^{2N} P_j Q_j + \sum_{j=2N+M+1}^{2N+2M} P_j Q_j \# \quad (5)$$

$$Ex_1(x,z) = \sum_{j=1}^{2N} Fx_j Q_j + \sum_{j=2N+M+1}^{2N+2M} Fx_j Q_j \# \quad (6)$$

$$Ez_1(x,z) = \sum_{j=1}^{2N} Fz_j Q_j + \sum_{j=2N+M+1}^{2N+2M} Fz_j Q_j \# \quad (7)$$

$$E_1(x,z) = \sqrt{E_{x1}(x,z)^2 + E_{z1}(x,z)^2} \# \quad (8)$$

where, P_j, Fx_j and Fz_j are, respectively, the potential and the radial- and axial-field coefficients calculated at the point A(x, z) due to the j^{th} ring charge [20–26]. The coordinates of the j^{th} ring charge and the coordinates of the point A(x, z) determine these coefficients.

Similarly, the potential $\varphi_2(x, z)$ and the radial- and axial-field components, $Ex_2(x, z)$, $Ez_2(x, z)$ and the absolute field $E_2(x, z)$ at any point A(x, z) in a gas medium are expressed by equations (9–12). They are the sum of the potentials and the radial-and axial-field components produced at this point by the ring charges of the rods and the solid dielectric:

$$\varphi_2(x,z) = \sum_{j=1}^{2N+M} P_j Q_j \# \quad (9)$$

$$Ex_2(x,z) = \sum_{j=1}^{2N+M} Fx_j Q_j \# \quad (10)$$

$$Ez_2(x,z) = \sum_{j=1}^{2N+M} Fz_j Q_j \# \quad (11)$$

$$E_2(x,z) = \sqrt{E_{x2}(x,z)^2 + E_{z2}(x,z)^2} \# \quad (12)$$

2.2. Positive corona onset voltage (COV) Criterion

When the applied voltage V and the corresponding electric field are high enough, an avalanche develops from free electrons available near the dielectric surface in the ionization zone. The avalanche size N_e is equal to $\exp\left(\int_l \bar{\alpha}(l)dl\right) [= \exp(K)]$, where K is an empirical constant that depends on the gas around the dielectric, and l is a field-dependent path that an electron avalanche can travel along inside an ionization zone. The dielectric surface influences the discharge inception by enhancing the local electric field. This field enhancement is caused by the difference in the dielectric permittivity of the dielectric material and the surrounding gas. At a critical value of the applied voltage, the critical avalanche size exp (K_0) results in a streamer discharge developing and transforming into discharges over the dielectric surface. The streamer discharge inception voltage is the positive COV; it is the peak value of the AC applied voltage, which results in the avalanche size of exp (K_0). The border of the ionization zone is defined where the effective ionization coefficient $\bar{\alpha}(l) \geq 0$ as $\bar{\alpha}(l) = \left(\alpha\left(\frac{E}{p}\right) - \eta\left(\frac{E}{p}\right)\right)$, E is the prevailing electric field on the field path l, p is the gas pressure, $\alpha\left(\frac{E}{p}\right)$ and $\eta\left(\frac{E}{p}\right)$ are Townsend's first ionization and the attachment coefficients as functions of *(E/p)*, respectively. Avalanche growth calculations considering the space charge field along a field line were done as explained before [28]. The avalanche starts to grow from the boundary of the ionization zone along a field line towards the higher voltage rod If the critical size of the avalanche along one of the field lines inside the ionization zone is obtained, the streamer inception criterion $\int_l \bar{\alpha}(l)dl \geq K_0$ is reached. Townsend's first ionization and attachment coefficients are given before for the gases under investigation; SF_6, CO_2 and N_2 [16], air [29], and argon [30].

Fig. 3 (a) shows a schematic representation of field lines and ionization zone boundaries at different applied voltage values V_1 and V_2, where $V_1 < V_2$, (V_2 = COV) for sample (b). Fig. 3 (b) shows the streamer inception integral, K calculated along different field lines at a given applied voltage. The streamer inception criterion is fulfilled at applied voltage with a maximum K value (K max) just equal to K_0. For gases under investigation, the inception integrals K_0 are taken as follows: For air, Raether suggested K_0 value of 18.42 [1,3,16] against 5, 10.5 and 15 for N_2, SF_6, and CO_2, respectively [16]. For argon, K_0 was considered equal to 10.2 [1]. For the SF_6-N_2 gas mixture, the value of K_0 is taken as $K_{0mixture} = kK_{0SF6} + (1-k)K_{0N2}$, where k is the per unit concentration value of SF_6 in the gas mixture [16].

3. Results and Discussion

3.1. Accuracy of the charge simulation

A set of checkpoints were selected midway between the boundary points on the rods and the dielectric surface to check the charge simulation's accuracy. The deviation of calculated potential from the applied voltage and the deviation angle of the field from being normal to the surface of the two rods were calculated at the checkpoints to assess how well the Dirichlet condition is satisfied at the two-rod surfaces. Also, to check how well the Neumann condition is met at the dielectric surface, the continuity of the electric potential and the normal electric field error were also calculated at the checkpoints.

The investigated samples have a length L of 200 mm, the radius of each rod, r = 8.5 mm. For sample (a), the solid dielectric cylinder radius range, $9.5 \leq R \leq 17.5$ mm, the gap length G = 4–8 mm, the relative permittivity ε_r = 2–6. For sample (b), R = 17.5 mm, G = 4 mm and ε_r = 4. and, S range, $1 \leq S \leq 8$ mm, corresponding to dielectric thickness t range, $8 \leq t \leq 1$ mm.

For sample (a): the simulation accuracy strongly depends on the number of simulation charges and their coordinates. The best accuracy is achieved for the investigated R range at arbitrary constant f_0 = 1.2 and the obtained simulation variables are given in Table 1. The total number of charges = 2 N + 2 M = 1248. For sample (b), in addition to the simulation variables given in Table 1 and the arbitrary constant f_0, the arbitrary constants f_1 = 1, and f_2 = 3 and the number of segments of ring charges simulating the dielectric surface, 2n = 14 segments. Hence, the total no of charges = 2 × (N + 2n × M), (=8684).

For rod-rod gaps without solid dielectric, the simulation is achieved by the charges at their locations in the sample (a). The total no of charges = 2 N, (=676 charges).

At the surface of the HV and grounded rods, the maximum percent potential errors and electric field deviation angles don't exceed: (i) at the surface of the flat parts, they are approximately zero, (ii) along the rounded part they are 0.004% and 0.16°, respectively and (iii) along the cylindrical part they are 0.06%, and 0.11°, respectively. At the dielectric surface, the maximum percent errors of the calculated potential and normal field values along the dielectric surface are 0.03 × 10^{-3} % and 0.06 %. The maximum percent potential errors and electric field deviation angle at the rods' surfaces remains the same for the rod-rod gap without a solid dielectric. In comparison with reasonable CSM accuracy published in the literature, potential errors on the electrode surface of less than 0.1% are considered reasonable for an accurate field calculation [21]. The maximum percent errors for the continuity of the electric potential and the normal electric field along the dielectric surface are 2 × 10^{-3} % and 1.5% [23], respectively. The calculated maximum

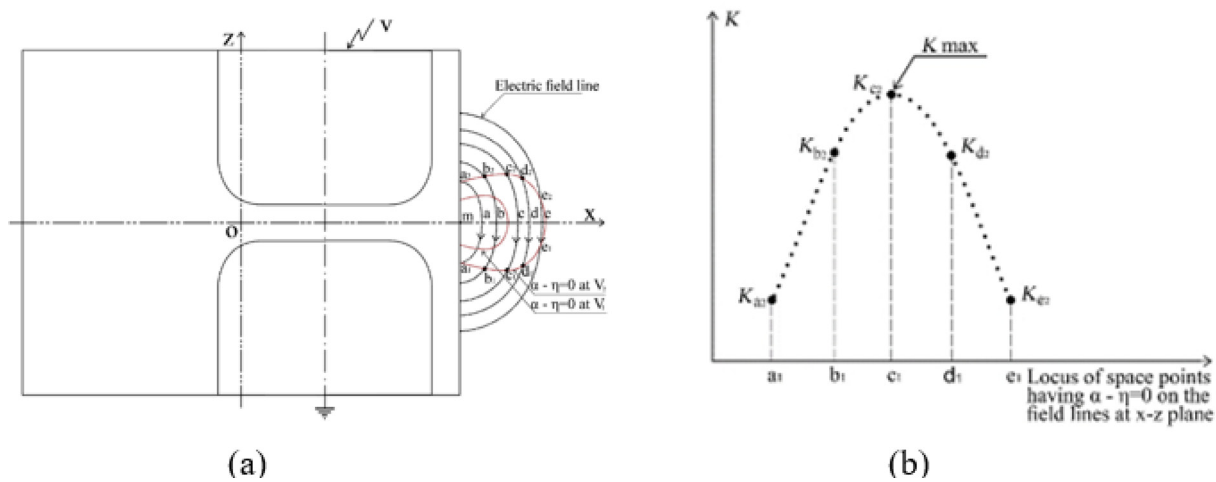

Fig. 3. (a) A schematic representation of field lines and the ionization zone borders at applied voltages V_1 and V_2, m is the maximum field point. (b) Variation of K at V_2 over field lines starting at a_1, b_1, c_1, d_1 and e_1 on the ionization zone border.

Table 1
Simulation variables obtained at the best accuracy of CSM for sample (a).

Simulation variables	HV rod or grounded rod			dielectric surface
	Flat part	Rounded part	Cylindrical part	
a_0 and A_0	a_0 = 0.014 r	a_0 = 0.01 r	a_0 = 0.054 r	A_0 = 0.048 R
a_1 and A_1	a_1 = 0.03 r	a_1 = 0.03 r	a_1 = 0.03 r	A_1 = 0.07 R
No. of charges	n_1 = 64	n_2 = 19	n_3 = 255	M = 286
Total no of charges	2 N + 2 M = 1248, N = n_1 + n_2 + n_3			

errors in the research work are much lower than those reported before in related calculations [23,27,31,32,33].

3.2. Electric field Distribution

Fig. 4 shows the calculation of electric field E using Eqs. (6–8) at an applied voltage V = 1 kV, G = 4 mm, ε_r = 4, S = 7 mm and t = 2 mm, and its components Ex and Ez along the HV rod, flat, rounded, and cylindrical surfaces. It is shown that the field is normal at the surface of the HV rod (Ex = 0, Ez = 0 at flat and cylindrical parts, respectively).

The field E is uniform at the flat portion with a value of 0.6245 kV/cm for sample (a) against 0.6249 kV/cm for sample (b) and very precisely coincides with the relation $E_{average} = [V / (\varepsilon_r \times G) = 0.625$ kV/cm], where, E_{max} = 0.8900 kV/cm for sample (a) against E_{max} = 0.8868 kV/cm for sample (b). i.e. the field enhancement factor for sample (a), $\xi = E_{max} / E_{average}$ = 1.425 against 1.419 for sample (b). These results show that shifting the axes affects the uniform field by 0.06 % and E_{max} by 0.36 % at the HV rod surface.

Fig. 5 (a) shows the 2D cut of the high field region in the x-z plane where V = 10 kV; the colour plot represents the calculated field in the surrounding gas for sample (b), (t = 2 mm corresponding to S = 7 mm). Potential and electric field distribution is calculated using Eqs. (9–12).

Normality for potential contours and field lines at the intersection points is achieved. Fig. 5 (b) shows the electric field calculation, E, along the solid dielectric surface at V = 10 kV for sample (a), (t = 9 mm, and t = 2 mm), as well as sample (b), (t = 2 mm). By shifting the axes distance S = 7 mm, Emax increased from 3.93 to 13.57 kV/cm, at the same V, with a subsequent decrease of the COV. For aligned axes, a decrease of the dielectric thickness, t, from 9 to 2 mm causes an enhancement of the electric field from

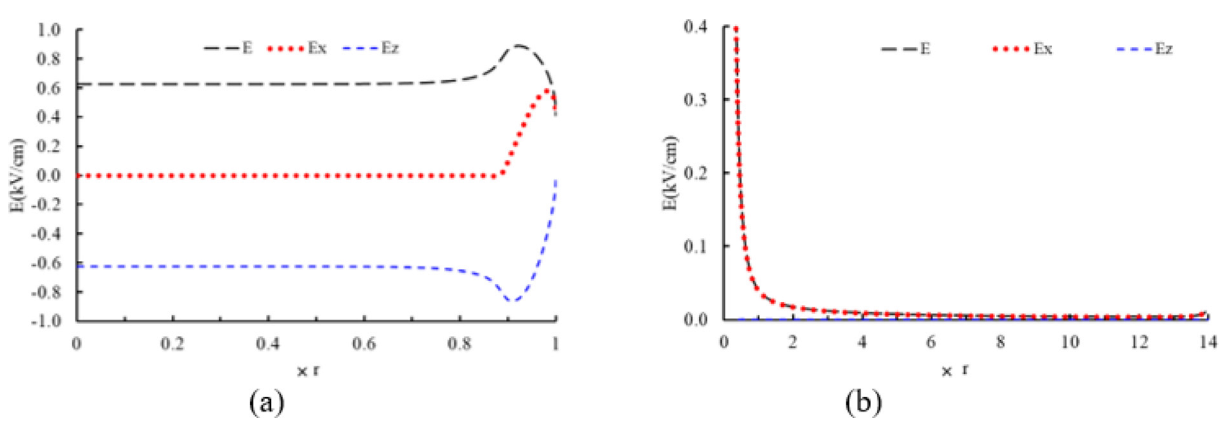

Fig. 4. Electric field distribution along the surface of the HV rod for sample (b), along the flat and rounded parts, (b) along the cylindrical part.

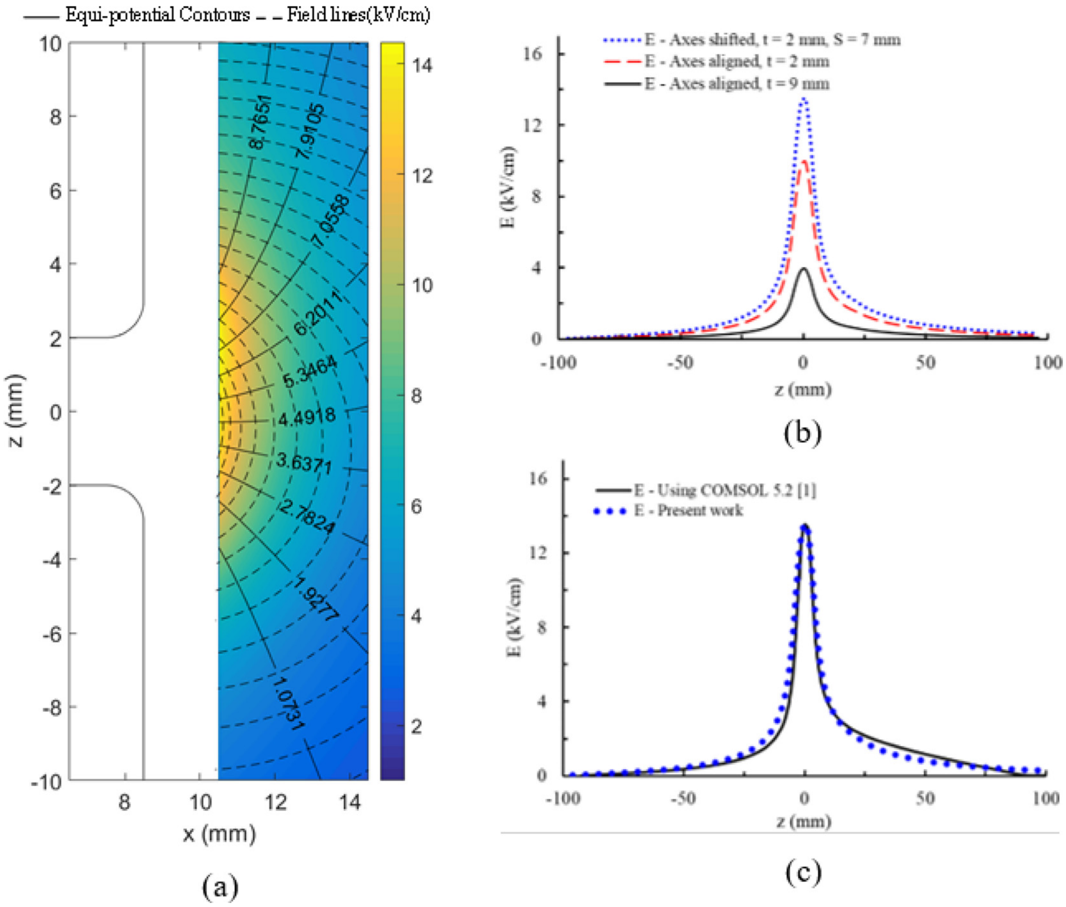

Fig. 5. (a) The 2D cut of the high field region - distribution of equipotential contours and field lines near the dielectric surface, for sample (b) at V = 10 kV. (b) E for samples (a), (t = 9 mm and t = 2 mm) and for sample (b), t = 2 mm. (c) E for sample (b), t = 2 mm compared with that obtained by COMSOL 5.2 [1].

3.93 to 9.79 kV/cm at the same V with a subsequent decrease of the COV. Fig. 5 (c) shows the calculated electric field along the surface of the solid dielectric, for sample (b), at V = 10 kV, ε_r = 4, S = 7 mm, R = 17.5 mm, and r = 8.5 mm, compared with the calculated values obtained before using software COMSOL 5.2 [1]. The maximum calculated field value is 13.565 against the previously calculated value of 13.563 kV/cm [1], i.e., they are nearly equal. This value is located at point m, shown in Fig. 3 (a), over the solid dielectric surface.

Fig. 6 shows the maximum p.u. field along solid dielectric surface related to the average field, (V/G), at G = 4 and 8 mm and ε_r of 2, 4 and 6, for sample (b), against t corresponding to varying values of S, (=9-t mm). The maximum p.u. field over the dielectric surface is less than the average for different values of t, S, G or ε_r. Positioning the electrodes closer to each other results in a higher electric field around the HV rod and a lower maximum p.u. field along the dielectric surface, corresponding to a higher maximum field over its surface, reducing COV. The increase of t (i.e. the decrease of S) and the decrease of ε_r cause a reduction in the maximum electric field, with an increase in the COV. (i.e. the best dielectric performance).

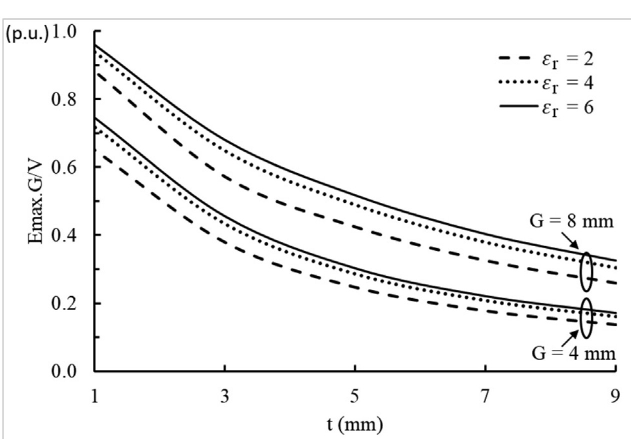

Fig. 6. Calculated maximum p.u. field along solid dielectric surface related to the average field V/G, for sample (b), against t, (S = 9- t mm).

3.3. Breakdown voltage for Rod-Rod gap without solid Dielectric

For the studied rod-rod gap without solid dielectric, the field enhancement factor ξ equals 1.425. So, the electric field is nearly uniform, and BD occurs directly [25]. The streamer inception criterion is used to calculate the breakdown voltage (BDV) of the rod-rod gap without solid dielectric. The peak voltage value of the HV AC cycle at which the first sustained discharge appears is referred to as the BDV. BDV is calculated for different SF_6-N_2 mixtures. The critical avalanche initiates at the maximum field point of the grounded rod and grows at the maximum field path towards the HV rod.

3.4. Positive corona onset voltage (COV) over the solid dielectric Cylinder

The peak voltage value of the HV AC cycle at which the first sustained discharge appears is referred to as COV. COV is calculated for different electronegative (SF_6, SF_6-N_2 mixtures, air, and CO_2) and electropositive (N_2 and argon) gases. The equivalencies between the COV of SF_6 and the proposed SF_6-N_2 mixtures were performed to allow confident use as alternative insulation to SF_6.

3.4.1. Influence of encasing rod-rod gap with solid dielectric on Emax at COV for shifted axes sample

Fig. 7 shows the calculated maximum electric field over the solid dielectric for sample (b), (R = 9 mm, r = 8.5 mm, S = 7 mm, G = 4 mm and ε_r = 4), and the same gap without the solid dielectric at streamer inception voltage in the surrounding N_2 and SF_6 gases against pressure. For N_2 gas at one bar, Emax values, 47.86 and 48.59 kV/cm are obtained by the present calculations and by COMSOL 5.2 [1], respectively, at COV of 32.7 kV, against (35.25 and 34.78 kV/cm) at BDV of 14.1 kV for the same gap without the solid dielectric. i.e. for sample (b), for N_2 gas, Emax is higher by about 36 %, and COV is higher than BDV without solid dielectric by about 132 % for present calculations. The current calculations for SF_6 gas at one bar, Emax, are (105.82, 97.25 kV/cm), at COV of 72.3 kV and BDV of 39.9 kV, with and without solid dielectric, respectively. i.e. Emax for SF_6 is higher by about 9%, and COV is higher than BDV without solid dielectric by 81 %. The field results over the solid dielectric surface agree well with previously published N_2 gas values; the maximum error does not exceed 1.5%. The calculated Emax at COV present a linear increase with the increase in gas pressure, and its value is always higher than Emax at BDV without the solid dielectric. Surface processes which may influence streamer inception are the attachment of free electrons or photoemission processes by the dielectric surface. The solid dielectric suppresses the growth of an avalanche compared to its growth in bulk gas with a subsequent increase of COV. It is proved that the maximum electric field required for streamer inception along the dielectric surface surrounded by N_2 or SF_6 is larger than that of the bulk gas alone [1].

3.4.2. Influence of gas pressure on COV in case of shifted axes sample

Fig. 8 (a) shows the present calculated COV compared with those measured [1] for different gases at p in the range 0.1–1 bar, for sample (b) (R = 17.5 mm, r = 8.5 mm, S = 7 mm, G = 4 mm and ε_r = 4). The COV results of SF6 have the highest values, while those of argon are the lowest. The COV values of air, CO_2 and N2 do not show significant differences. Error bars for N2, air, and CO_2 were in the range of (10–15) % [1]. The calculated COV values present a linear increase with the increase in gas pressure in all gases. The calculated values agree well with a maximum error of less than 10 % from published measured values [1]. Fig. 8 (b) shows the calculated COV values for different SF_6- N_2 gas mixtures compared to practical values [1], for sample (b) (S = 7 mm, t = 2 mm). The COV values increase linearly with an increase in pressure for all gas mixtures. The calculated COV values over the solid dielectric surface show a good agreement with a maximum error of less than 10 % from previously measured values.

Fig. 9 shows the calculated COV values over the solid dielectric surface and the BDV of the rod-rod gap without solid dielectric against SF_6 percentage content at different pressures for sample (b), (R = 9 mm, r = 8.5 mm, S = 7 mm and ε_r = 4). The COV values increase with the increased SF_6 gas content in the gas mixture. The rate of increase starts to reduce at a certain content (20%) and tends to saturate in the 80% –100% range. COV values for gases SF_6, N_2, and SF_6 - N_2 mixture increase directly as gas pressure increases. The COV of the gas mixture should be the weighted value of each gas's partial pressure or volume ratio. However, the DIV values of the SF_6 - N_2 mixture are higher than the linear combination of those of SF_6 and N_2. This phenomenon in gas mixtures is called the synergistic effect. The strongest synergistic effect occurs when the percentage content of SF_6 lies between 20% and 30%, as previously mentioned [34].

3.4.3. Influence of gas pressure on COV in case of common axis sample

The streamer criterion fails to accurately predict the COV at p higher than 3 bar, for strongly electronegative gases and their mixtures with other gases [18]. Hence, the COV is calculated using streamer criterion up to 3 bars for standard gas mixture option 50% SF_6 + 50% N_2 [11] and the strongest synergistic 20% SF_6 + 80% N_2 mixtures [34] for comparison against COV of pure SF_6 and pure N_2.

Fig. 10 shows how the calculated COV over the solid dielectric surface for the common axis, sample (a), (r = 8.5 mm, R = 17.5 mm, G = 4 mm and ε_r = 4), increases with the increase in gas pressure. Both COV and BDV values increase as the gas pressure increases. The equivalencies between the COV of SF_6 and the proposed SF_6- N_2 mixtures to allow confident use as alternative insulation to SF_6 are shown in the figure. At constant pressure, 2.5 bar, those mixtures of 50% SF_6 + 50% N_2 and 20% SF_6 + 80% N_2 have 0.86 and 0.69, respectively, of the COV for pure SF_6. To reach the same COV with pure SF_6, the pressure of the SF_6- N_2 mixture should increase, as shown in the figure. Mixtures of equal amounts of SF_6 and N_2 at 2.5 bars exhibit the same COV as pure SF_6 when operated at 15% higher pressure, as shown in the figure and as mentioned before [11]. In addition, it has 0.86 the dielectric strength of pure SF_6 at the same pressure, which is nearly equal to the published value for bulk gas in a uniform field at few bars, (=0.88) [11].

3.4.4. Influence of dielectric thickness on COV in case of common axis sample

Fig. 11 shows how calculated COV values over the solid dielectric surface for the aligned axis, (sample (a)), increase with the increase in dielectric thickness, t at one bar. COV values increase as the dielectric thickness, t, increases. The equivalencies between the COV of SF_6 and the proposed SF_6-N_2 mixtures to allow confident use as alternative insulation to SF_6 are obtained from the shown figure. At constant dielectric thickness, t = 5 mm, COV of SF_6 = 133.6 kV, COV of mixtures of 50% SF_6 + 50% N_2 and 20% SF_6 + 80% N_2 related to COV of SF_6 are 0.81 and 0.7, respectively. To reach the same COV with pure SF_6, the dielectric thickness, t, for the two mixtures should increase to 6.45 and 7.75 mm, respectively. The calculated BDV values without solid dielectric are also shown at the extension of COV relations.

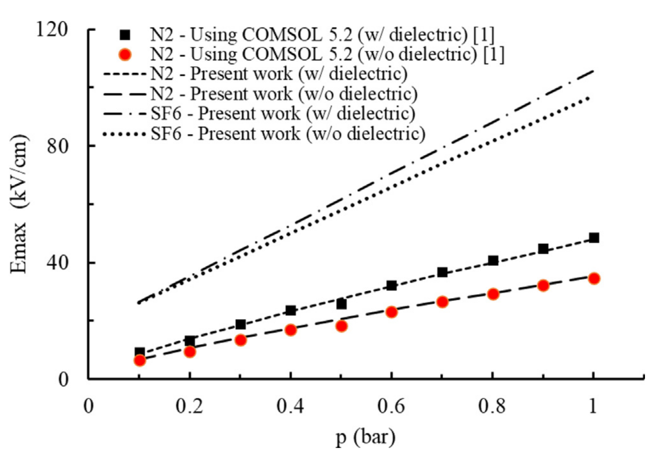

Fig. 7. Calculation of maximum electric field over the solid dielectric of sample (b), for gases N_2 and SF_6 at COV and BDV with and without solid dielectric, respectively, compared with those obtained by COMSOL 5.2 [1] in case of N_2.

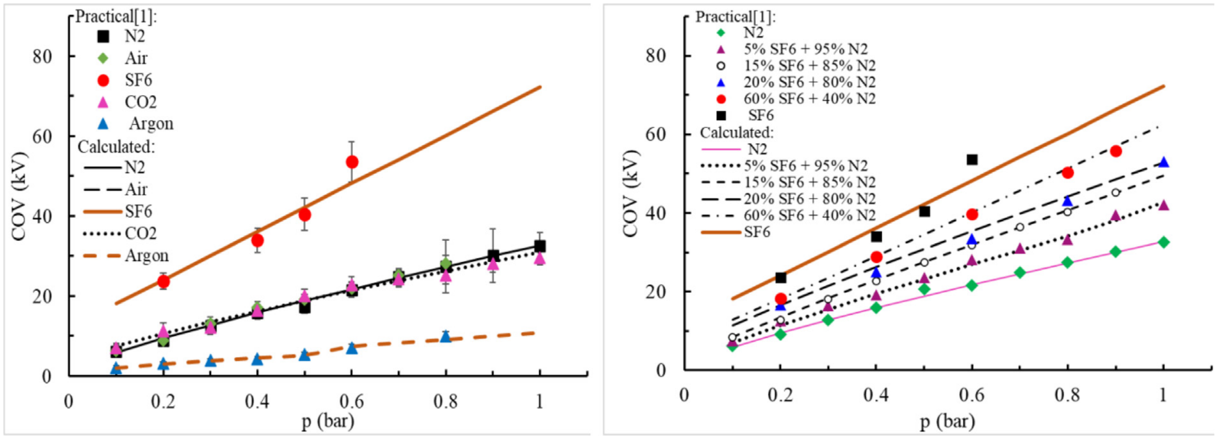

(a) (b)

Fig. 8. Calculated COV values against p compared to practical values [1], for sample (b); (a) for different gases, (b) for different SF_6- N_2 gas mixtures.

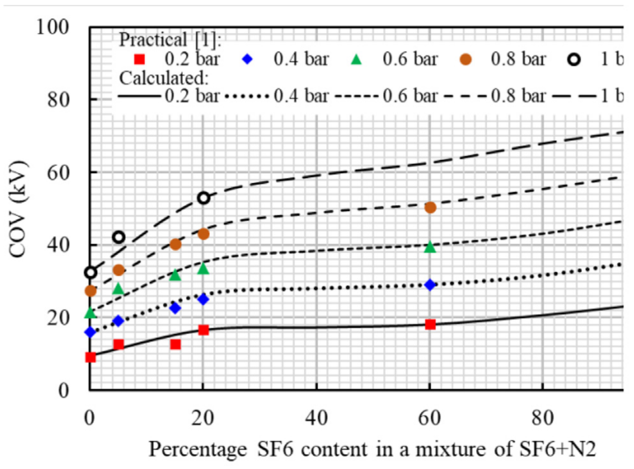

Fig. 9. Calculated COV against percentage SF_6 content in a mixture of SF_6 + N_2 at different p for sample (b).

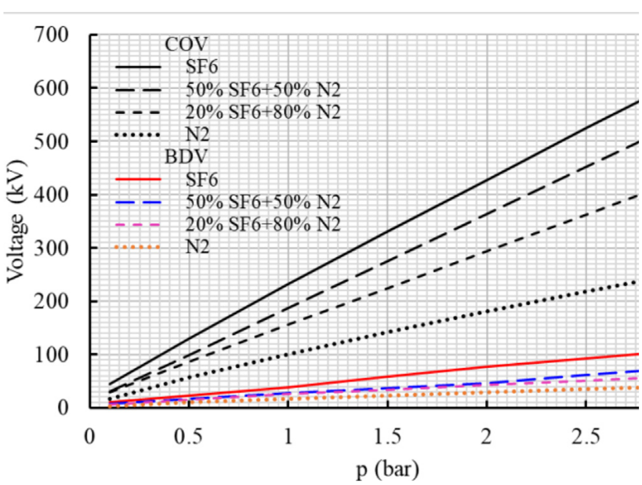

Fig. 10. Calculated COV for sample (a) and BDV without solid dielectric against p.

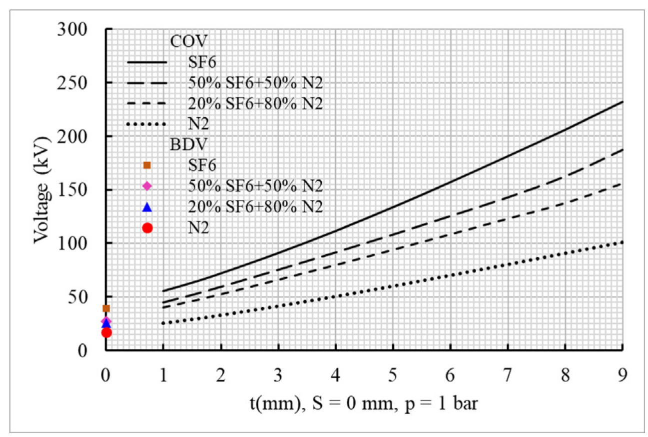

Fig. 11. Calculated COV for sample (a), against t at p = 1 bar, r = 8.5 mm, G = 4 mm, ε_r = 4, and BDV without solid dielectric.

4. Conclusion

The presented analysis calculates the electric field accurately for a rod-rod gap and rod-rod gaps encased with a solid dielectric cylinder with a common axis and axes offset by a distance. Positioning the rods closer to each other results in a higher maximum field along the solid dielectric surface, reducing the COV. The shift in rod-rod gap-axis out from the dielectric cylinder axis also causes an electric field enhancement, with a subsequent decrease of the COV. As the solid dielectric thickness increases and the relative permittivity decreases, the lowest value of the maximum electric field is obtained, and the COV increases (i.e. best dielectric performance). It is proved that the electric field required for streamer inception along the dielectric surface where the surrounding gas is N_2 or SF_6 is larger than in bulk gas alone, corresponding to higher COV than BDV without the solid dielectric. The field results over the solid dielectric surface agree well with previously published values; the maximum error does not exceed 1.5%. The calculated COV values present a linear increase with an increase in gas pressure or dielectric thickness. The calculated COV values agree well with the published measured values where the maximum deviation does not exceed 10%. The equivalencies between the COV of

SF_6 and the proposed SF_6 - N_2 mixture are investigated to allow confident use as alternative insulation to SF_6 in the presence of a solid dielectric cylinder. The amount of SF_6 using 50% SF_6 – 50% N_2 mixture as a surrounding gas to cylindrical solid dielectric encasing stressed rod-rod gap can be reduced significantly without losing much dielectric strength.

Declaration of Competing Interest

The authors declare that they have no known competing financial interests or personal relationships that could have appeared to influence the work reported in this paper.

References

[1] A.V. Chvyreva, "Creeping sparks: a study on surface discharge development" Phd Thesis, Eindhoven University of Technology, 2016.
[2] Chvyreva AV, Pemen AJM, Christen T. Influence of SF_6 admixtures to nitrogen on electrodeless streamer inception at an epoxy resin surface. IEEE Trans Dielectr Electr Insul 2016;23(3):1683–9.
[3] A. Pedersen, T. Christen, A. Blaszczyk and H. Boehme, "Streamer inception and propagation models for designing air insulated power devices" CEIDP' 09 Conf. Materials, pp. 604–607, Nov. 2009.
[4] A. Chvyreva, S. Pancheshnyi, T. Christen and A. J. M. Pemen, "Raether-Meek criterion for prediction of electrodeless discharge inception on a dielectric surface in different gases" Journal of Physics D: Applied Physics, Jan. 2018.
[5] Sudarshan TS, Dougal RA. Mechanisms of surface flashover along solid dielectrics in compressed gases: a review. IEEE Transaction on Electrical Insulation Oct. 1986;21(5):727–46.
[6] C. Tran Duy, N. Bonifaci,_, A. Denat, O. Lesaint, L. Caliap, A. Girodet, B. Gelloz, P. Ponchon, "Partial discharges at a triple junction metal/solid insulator/gas and simulation of inception voltage" Journal of Electrostatics, Vol. 66, 319–327, May 2008.
[7] Hara M, Kurihara T, Kozuru S, Suehiro J, Hayashi N. Estimation of partial discharge onset characteristics in gases around a triple junction. Electr Eng Jpn 2003;144:1–11.
[8] N.G. Trinh, "Failure mechanisms of gas insulation and at gas–insulator interface: their influence on gas-insulated equipment" in: L.G. Christophorou, I. Sauers (Eds.), Gaseous Dielectrics VI, New York, pp. 517–529, 1991.
[9] Ambo NF, Zainuddin H, Kamarudin MS, Wari JM, Zahari A. AC breakdown behavior of SF_6/N_2 gas mixtures under non-uniform field electrode configurations. TELKOMNIKA Oct. 2019;17(5):2451–6.
[10] Christophorou LG, Van Brunt RJ. SF_6/N_2 mixtures basic HV insulation properties. IEEE Transaction on Dielectrics and Electrical Insulation 1995;2 (5):952–1003.
[11] L. G. Christophorou, J. K. Olthoff and D. S. Green, "Gases for Electrical Insulation and Arc Interruption: Possible Present and Future Alternatives to Pure SF_6" National Institute of Standards and Technology, Technical Note 1425, 1997.
[12] Kawamura T, Matsumoto S, Hanai M, Murayama Y. In: SF_6/N_2 Mixtures for HV Equipment and Practical Problems. New York, NY, USA: Kluwer Academic/ Plenum Publishers:; 1998. p. 333–43.
[13] M. M. El-Bahy, "Onset Voltage of Corona in SF_6-N_2 Mixtures" 2000 IEEE Conference on Electrical Insulation and Dielectric Phenomena, No. l, pp. 393-396, Oct. 2000.
[14] Duzkaya H, Dincer MS, Hiziroglu HR. Calculation of Partial Discharge Inception Voltages in Ultradilute SF_6+N_2 Gas Mixtures. In: 2009 Annual Report Conference on Electrical Insulation and Dielectric Phenomena. p. 531–4.
[15] Beroual A, Khaled U, Coulibaly ML. "Experimental Investigation of the Breakdown Voltage of CO_2, N_2, and SF_6 Gases, and CO_2–SF_6 and N_2–SF_6 Mixtures under Different Voltage Waveforms" Energies 11. No 2018;4:902.
[16] N. H. Malik and A. H. Qureshi, "Breakdown Gradients in SF_6-N_2, SF_6-Air and SF_6-CO_2 Mixtures" in IEEE Transactions on Electrical Insulation, Vol. EI-15, No. 5, pp. 413-418, Oct. 1980.
[17] Tian S, Zhang X, Cressault Y, Hu J, Wang B, Xiao S, et al. Research status of replacement gases for SF_6 in power industry. AIP Adv May 2020;10(5).
[18] L. Chen, P. Widger, C. Tateyama, A. Kumada, H. Griffiths, K. Hidaka and A. Haddad, "Breakdown Characteristics of CF3I/CO_2 gas mixtures under fast impulse in rod-plane and GIS geometries" In Proceedings of the 19^{th} International Symposium on High Voltage Engineering, Pilsen, Czech Republic, Aug. 2015.
[19] P. Simk and N. Ranjan, "Dielectric strength of C5 Perfluoroketone" In Proceedings of the 19^{th} International Symposium on High Voltage Engineering, Pilsen, Czech Republic, Aug. 2015.
[20] Singer H, Steinbigler H, Weiss P. A charge simulation method for the calculation of high voltage fields. *IEEE* Trans PAS 1974;93:1660–8.
[21] Malik NH. A review of the charge simulation method and its applications. IEEE Trans Electr Insul Feb. 1989;24(1):3–20.
[22] Abdel-Salam M, Turky A, Hashem A. The onset voltage of coronas on bare and coated conductors. J Phys D: Applied Physics 1998;31(19):2550–6.
[23] El-Bahy M, Abouelatta M. Onset voltage of negative corona on dielectric-coated electrodes in air. J Phys D Appl Phys 2005;38(13):3403.
[24] El-Bahy M. A numerical modelling of microdischarge threshold in uniform electric fields. J Phys D: Appl Phys Dec. 2005;38(1):103–12.
[25] Bilbao J, Bravo E, García O, Rebollar C, Varela C. Numerical Analysis of Electromagnetic Fields. Switzerland: Book published by Springer Nature Switzerland AG; 2021.
[26] M. Abdel-Salam, H. Anis, A. El-Morshedy, R. Radwan, "High-Voltage Engineering: Theory and Practice (2nd ed.)" CRC Press, 2000.
[27] El Bahy M, Ward SA, Morsi R, Badawi M. Onset voltage of a particle-initiated negative corona in a co-axial cylindrical Configuration. J Phys D: Applied Physics 2013;46(4):045205.
[28] H. Parekh and K. D. Srivastava, "Effect of Avalanche Space Charge Field on the Calculation of Corona Onset Voltage" in IEEE Transactions on Electrical Insulation, Vol. EI-14, No. 4, pp. 181-192, Aug. 1979.
[29] Iravani MR, Raghuveer MR. Accurate field solution in the entire interelectrode space of a rod–plane gap using optimized charge simulation. IEEE Transactions on Electrical Insulation, Vol EI-17, No Aug 1982;4:333–7.
[30] M. Abouelsaad and M. El-Bahy, "Accurate field computation of needle–plane gaps using an optimized charge simulation method" 2000 IEEE Conference on Electrical Insulation and Dielectric Phenomena, Canada, Vol. 2, pp. 506-509 Oct. 2000.
[31] El-Bahy M. In: Onset voltage of negative corona in point-cup gaps. Staffordshire University; 2002. p. 159–63.
[32] El-Hawary HH, Abdel-Salam M, Hashem A-A-R, Turky A-H-A. Inception Voltage of Burst Pulses, Onset Streamers, and Positive Glow in Short Rod-to-Plane Gaps. IEEE Trans Plasma Sci June 2021;49(6):1763–75.
[33] Radjenovic R, Radjenovic M, Klas B, Bojarov M, Matejcik A, Stefan,. The breakdown mechanisms in electrical discharges: The role of the field emission effect in direct current discharges in microgaps. Acta Physica Slovaca 2013;63 (3):105–205.
[34] Qin Z, Zhang C, Zheng Y, Zhou W, Yang S. Insulation Properties of SF_6/N_2 Gas Mixtures Under High Pressure and Low Ratio. In: 2017 IEEE Electrical Power and Energy Conference (EPEC). p. 1–4.

Mohamed Ibrahim Awaad : Mobile: +(202)- 107579039, **Affiliation:** Department of Electrical Engineering, Benha Faculty of Engineering, Benha University, Benha 13511, Egypt.

Ahmed Nasr Eldeen: Mobile: +(202)- 1062083713, **Affiliation:** Department of Electrical Engineering, Benha Faculty of Engineering, Benha University, Benha 13511, Egypt.

Mahmoud Elbahy: Mobile: +(202)- 1003706442, **(**Professor of High Voltage Engineering), **Affiliation:** Department of Electrical Engineering, Benha Faculty of Engineering, Benha University, Benha 13511, Egypt.